Journal of Geophysical Research: Atmospheres

RESEARCH ARTICLE
10.1029/2018JD028674

Convective Influence on the Humidity and Clouds in the Tropical Tropopause Layer During Boreal Summer

Rei Ueyama[1,2], Eric J. Jensen[1], and Leonhard Pfister[1]

[1]NASA Ames Research Center, Moffett Field, CA, USA, [2]Bay Area Environmental Research Institute, Moffett Field, CA, USA

Key Points:
- Convection moistens (0.6 ppmv) and increases clouds (170%) in the summer TTL
- Convection is important for H_2O and cloud maxima over the Asian monsoon
- Convective ice has negligible impact on TTL humidity and clouds in summer

Correspondence to:
R. Ueyama,
rei.ueyama@nasa.gov

Citation:
Ueyama, R., Jensen, E. J., & Pfister, L. (2018). Convective influence on the humidity and clouds in the tropical tropopause layer during boreal summer. *Journal of Geophysical Research: Atmospheres*, *123*, 7576–7593. https://doi.org/10.1029/2018JD028674

Received 16 MAR 2018
Accepted 21 JUN 2018
Accepted article online 2 JUL 2018
Published online 17 JUL 2018

Abstract The impact of convection on the humidity and clouds in the tropical tropopause layer (TTL) during boreal summer 2007 is investigated in simulations of detailed cloud microphysical processes and their effects on the water vapor (H_2O) profile along backward trajectories from the 379 K potential temperature (100-hPa pressure) surface. Convective influence is determined by tracing the trajectories through time-dependent fields of satellite-based convective cloud top height. The simulated H_2O mixing ratios at the 100-hPa level and cloud occurrence fractions in the middle to upper (16–18 km) TTL exhibit a pronounced maximum over the Asian monsoon region as in observations; these local enhancements are virtually absent in the simulation without convection, indicating that convection is the dominant driver of the localized H_2O and cloud maxima in the Asian summer monsoon region. Convection moistens the 100-hPa level by 0.6 ppmv (~15%) averaged over the 10°S–50°N domain and increases tropical (10°S–30°N) mean cloud occurrence in the middle to upper TTL by ~170%. Nearly all of the convective enhancements in H_2O and clouds are due to the effect of convective saturation; convectively detrained ice crystals have negligible impact. Parcels are most frequently hydrated by deep convection in the southern sector of the Asian monsoon anticyclone and subsequently dehydrated downstream of convection to the west, shifting the locations of final dehydration northwest of the cold temperature region in the northern Tropics. Infrequent, extreme deep convective systems (cloud tops exceeding 380 K) have a disproportionately large effect on TTL humidity and clouds.

1. Introduction

Global stratospheric water vapor (H_2O) is primarily controlled by the troposphere-to-stratosphere transport of H_2O through the tropical tropopause layer (TTL: e.g., Fueglistaler et al., 2009, and references therein) and the oxidation of methane in the stratosphere. The large-scale cold point tropopause temperature field in the TTL plays a predominant role in driving seasonal and interannual variations in stratospheric-entry H_2O (Mote et al., 1996; Randel et al., 2006), but processes involving convection, gravity waves, and cirrus cloud microphysics also modulate TTL humidity (Bonazzola & Haynes, 2004; Dessler et al., 2007, 2016; Dinh & Fueglistaler, 2014; Gettelman et al., 2002; Jensen & Pfister, 2004; Liu et al., 2010; Schiller et al., 2009; Schoeberl & Dessler, 2011; Schoeberl et al., 2014, 2015, 2016, 2018; Ueyama et al., 2014, 2015) and may significantly impact stratospheric humidity. Accurate simulations of H_2O in the TTL, and ultimately in the stratosphere, are critical for reliable climate projections, but current global climate models are limited in their representation of the physical processes controlling H_2O transport through the TTL (Gettelman et al., 2009, 2010), such as deep convective transport of H_2O and ice.

Overshooting deep convection is capable of transporting H_2O across the tropopause into the tropical lower stratosphere (Chaboureau et al., 2007; Corti et al., 2008; Danielsen, 1993; Dessler & Sherwood, 2004; Dessler et al., 2007; Grosvenor et al., 2007; Hanisco et al., 2007; Kley et al., 1982; Kritz et al., 1993; Pfister et al., 1993; Schiller et al., 2009; Sherwood & Dessler, 2001), but its overall impact on the global stratospheric H_2O budget may be insignificant (Schoeberl et al., 2014, 2018). Additionally, whether or not convectively detrained ice crystals can significantly moisten the lower stratosphere is still an open question (Dessler et al., 2007, 2016; Schoeberl et al., 2014; Ueyama et al., 2015).

Convective moistening appears to play a role in the formation of the localized H_2O maximum near the tropopause over the boreal summer monsoon regions (Dessler & Sherwood, 2004; Randel et al., 2001; Schwartz et al., 2013; Smith et al., 2017), but sources and pathways of convective transport on this regional

scale are not well understood. In particular, remaining questions regarding the Asian monsoon H_2O enhancements include (i) the relative importance of convective source of H_2O from the Tibetan Plateau and southern slope of the Himalayas (Bannister et al., 2004; Bergman et al., 2012; Fu et al., 2006; Lelieveld et al., 2007; Wright et al., 2011) versus Bay of Bengal and South China Sea (Devasthale & Fueglistaler, 2010; James et al., 2008; Park et al., 2007; Tissier & Legras, 2016) and (ii) the degree to which moist air detrained from these convective systems bypasses the cold temperature region of the western tropical Pacific (Gettelman et al., 2004; James et al., 2008; Wright et al., 2011). Trajectory studies by James et al. (2008) and Schoeberl et al. (2013) have independently concluded that the enhanced H_2O over the Asian monsoon region at the 100-hPa level is not due to convective moistening, but instead controlled by large-scale transport through relatively warm temperatures. Randel et al. (2015) showed that dehydration in large-scale TTL cold anomalies associated with deep convection may be as important as (or more important than) convective hydration itself for controlling the subseasonal variability in stratospheric H_2O in the boreal summer Asian and North American monsoon regions.

The purpose of this study is to evaluate the role of convection on the humidity and clouds in the TTL during boreal summer. We focus on the boreal summer because stratospheric humidity during this season appears to be disproportionately set by TTL conditions over the southeast Asian monsoon region (Fueglistaler et al., 2005), which does not necessarily coincide with the minimum temperature region further south and southeast; this suggests that TTL humidity may be partially decoupled from tropical tropopause temperatures in boreal summer unlike in boreal winter. This study also aims to clarify the questions related to the Asian summer monsoon discussed above. Section 2 describes the observations that motivate this study and the model setup. Section 3 presents the simulation results and quantifies the impact of convection on the 100-hPa level H_2O and TTL cirrus cloud occurrence fraction. Convective sources of H_2O and clouds, as well as transport pathways of air parcels in the Asian monsoon region, are also analyzed. A summary of the results and their implications are discussed in section 4.

2. Data and Methods

The combined trajectory and cloud model approach used in this study follows the method described in Ueyama et al. (2015) with minor modifications to the global convective cloud top height estimates and cloud microphysical modeling. It is broadly based on the approach used in Jensen and Pfister (2004). Briefly, 60-day backward diabatic trajectories are launched once a day over a 7-day period centered on 3 August 2007 (i.e., a total of seven sets of trajectories ending on each day between 31 July and 6 August 2007) from a 2° latitude × 2° longitude grid of points in the 10°S–50°N domain at 379 K potential temperature level (which corresponds to ~100-hPa level). 3 August was chosen as the central trajectory starting date because the 7-day mean, 100-hPa level H_2O field in the Tropics centered on that date exhibits maximum (spatial) correlation with the seasonal (June–August 2007) mean H_2O field based on Microwave Limb Sounder (MLS; Read et al., 2007), shown in Figure 1. The two most prominent features are the anomalously moist air within the upper-level anticyclonic circulation in the Northern Hemisphere defined as the Asian and North American summer monsoon regions.

The diabatic trajectories are calculated using horizontal wind data from the 6-hourly interim reanalysis of the European Centre for Medium-range Weather Forecasts (ERA-Interim: Dee et al., 2011). The interpolation technique of Kim and Alexander (2013) is applied to the ERA-Interim temperature and horizontal wind data to recover the degraded wave-driven variability in the ERA-Interim data in the TTL, but only the power of the temperature data is enhanced due to uncertainties in the power amplification factor for the wind fields. The diabatic vertical motion is determined by offline calculations of tropical radiative heating rates of Yang et al. (2010) merged with extratropical radiative heating rates from ERA-Interim averaged over the three boreal summer months (June, July, and August) in 2007. Yang et al. (2010) heating rates based on satellite observations of cloud fields are only available as monthly averages given the need to aggregate the sparse satellite cloud measurements. In reality, the heating rates and vertical motions vary on much shorter time scales because the cloud fields are highly variable. However, vertical transport through the TTL is slow (mean ascent rates of ~0.3 mm s^{-1}), and its cumulative impact on TTL humidity is on the order of weeks. Given the sensitivity of the diabatic heating rates to clouds both locally and at lower altitudes (Corti et al., 2006; Hartmann et al., 2001) and the uncertainties in global model representations of clouds that lead to large differences

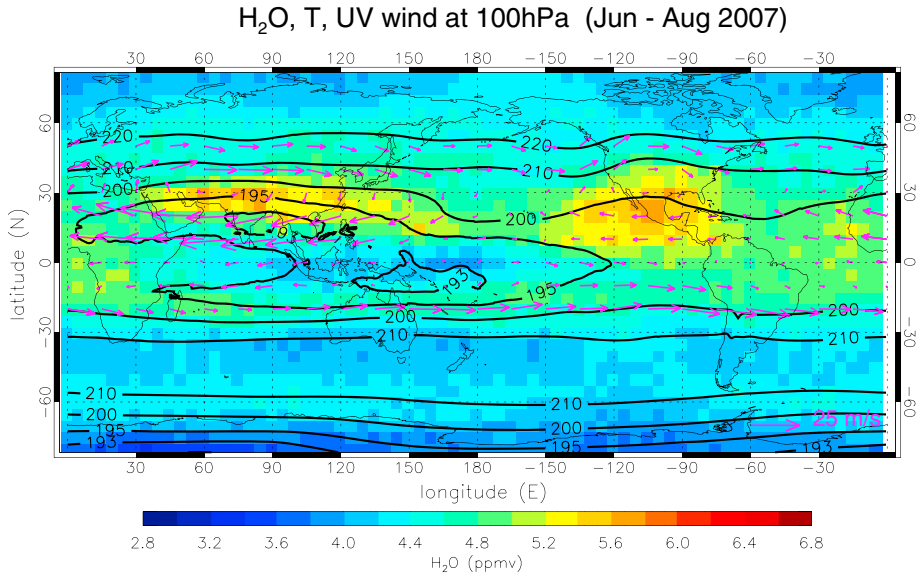

Figure 1. Boreal summer (June–August 2007) mean Microwave Limb Sounder H_2O mixing ratios (ppmv; color shading) and ERA-Interim temperatures (K; contours) and horizontal winds (m s^{-1}; vectors) at the 100-hPa level.

in TTL radiative heating rates in the reanalysis products (Randel & Jensen, 2013), the observation-based Yang et al. (2010) heating rates are likely to be more suitable for this study. Ueyama et al. (2015) found that the use of Yang et al. (2010) heating rates, as opposed to ERA-Interim heating rates, resulted in ~20% increase in the tropical mean H_2O at the 100-hPa level and ~5% decrease in TTL cloud occurrence during boreal winter. Radiative heating rates in the TTL during boreal summer are ~50% smaller (i.e., weaker ascent above the level of zero radiative heating) than those during boreal winter, and thus, the choice of heating rate data has less impact on the boreal summer results, as discussed in section 4. Horizontal and vertical dispersion rates of the trajectories that translate into trajectory path errors are on the order of 3° d^{-1} and 2–3 hPa d^{-1} near the tropical tropopause, respectively, but the averaging of thousands of trajectories as done here should provide statistically reliable information of parcel source and pathway distributions (Bergman et al., 2016).

Next, we simulate the evolution of ice clouds including nucleation, deposition growth, sedimentation, and sublimation of ice crystals in one-dimensional (vertical) space along each trajectory path. Time-height "curtains" of temperature and heating rate are constructed by extracting their vertical profiles (350–430 K potential temperature levels) versus time (0–60 days) along the trajectories from their respective data sets. The lack of vertical wind shear in the curtain approach is an obvious limitation, but it should not significantly impact the results given that a typical cloud lifetime is about 1–2 days (Jensen et al., 2011), as discussed in Ueyama et al. (2015). Cirrus cloud processes are simulated along the trajectory curtains using a Lagrangian cloud microphysical model initialized with 7-day mean MLS H_2O data averaged over 5° latitude × 5° longitude bins on the earliest day of the trajectories; the results are not sensitive to the initial H_2O distribution. The model simulates homogeneous ice nucleation when the ice saturation ratio, calculated using the temperature curtains, exceeds a threshold of ~1.6 (Koop et al., 2000); thousands of individual ice crystals are tracked, allowing for a proper representation of the ice size distribution. The heating rate curtains are used to diagnose the vertical (cross-isentropic) transport of ice crystals and H_2O through the depth of the TTL following the trajectory path, and thus, this approach properly treats the vertical redistribution of water by clouds. The model calculates vertical profiles of H_2O and clouds at each time step along the 60-day trajectories.

High-frequency gravity waves with periods less than 1/2 day are not resolved in the reanalysis data even after applying the Kim and Alexander (2013) interpolation to the reanalysis fields. These waves affect both the minimum temperatures experienced by the parcels along their trajectories as well as cloud microphysical properties such as ice number concentrations and ice crystal size distributions produced by homogeneous ice nucleation (Dinh et al., 2016; Jensen & Pfister, 2004; Schoeberl et al., 2015). Several studies have shown

that high-frequency gravity waves have minimal impact on TTL humidity (Fueglistaler & Baker, 2006; Schoeberl et al., 2014, 2015; Ueyama et al., 2015) and small to moderate effect on cloud occurrence (Schoeberl et al., 2015, 2016; Ueyama et al., 2015). Here we add climatological mean high-frequency gravity waves to the trajectory temperature curtains following Jensen and Pfister (2004), but their frequencies extended to the Brunt-Väisälä frequency.

In the final step, we compare the simulated H_2O mixing ratios at 100 hPa on the final day (start date of the backward trajectories) and cloud fraction during the last 30 days of the 60-day integration period with corresponding satellite observations. The model H_2O values are properly convolved with the MLS averaging kernels before comparing with MLS data, following the description of the averaging kernels for MLS version 3.3 profiles in the Data Quality and Description Documentation. The MLS averaging kernel is not applied to the model H_2O values when comparing between simulations (e.g., for quantifying the impact of convection on 100-hPa H_2O field). The typical single-profile precision for MLS H_2O at the 100-hPa level is 15% (~0.5 ppmv).

The simulated cloud occurrence frequencies are compared with those estimated from the Cloud-Aerosol Lidar with Orthogonal Polarization (CALIOP) instrument onboard the Cloud-Aerosol Lidar and Infrared Pathfinder Satellite Observations (Winker et al., 2009) satellite. Version 4 CALIOP Level 2 Cloud Layer data are screened to exclude integrated attenuated backscatter values less than 0.001 and greater than 0.019 to avoid noise problems at the low end and optically thick convective clouds at the high end. We also restrict ourselves to nighttime data when the CALIOP cloud detection extinction coefficient threshold is lower due to the larger signal-to-noise ratio. Model cloud ice with extinction greater than 5×10^{-3} km^{-1}, calculated based on ice crystal size distribution, are used to compare with CALIOP data. The simulated and observed tropical mean cloud occurrence fractions are compared in the mid to upper (16–18 km) TTL. The model is best equipped to calculate clouds formed in situ by cooling due to waves and large-scale motion. Thus, model cloud statistics are particularly robust in the middle to upper TTL where the assumption of simple isentropic flow with vertical motion balanced by radiative heating is reasonable. In the lower TTL near the model's bottom boundary, convective motions and latent heating complicate the balance.

Convective influence of air parcels is treated by tracing the trajectories through time-dependent (3-hourly) fields of convective cloud top height based on rainfall measurements, geostationary infrared satellite imagery, and temperature analyses (Bergman et al., 2012; Pfister et al., 2001). The estimated cloud top heights are adjusted for known biases in infrared cloud top temperature (Minnis et al., 2008; Sherwood et al., 2004) by uniformly adding 1 km to the cloud top altitudes. The analysis temperature profiles are modified above the analysis tropopause by calculating a profile that is a mixture of (70%) tropopause air and (30%) environmental air, broadly consistent with the observed cooling effect of convection near the tropopause (Chae et al., 2011; Selkirk, 1993; Sherwood et al., 2003). The altitude of the infrared brightness temperature in the modified temperature profile is then defined as the cloud top altitude. Precipitation estimates from Tropical Rainfall Measuring Mission and Global Precipitation Measurement are used to distinguish convective clouds from in situ-formed cirrus clouds. Rainfall thresholds used for identification of convection (i.e., 0.9 and 1.5 mm h^{-1} over land and ocean, respectively) are adjusted to statistically match combined CloudSat and CALIOP observations of deep convection cloud top height frequency. A comparison of convective cloud top heights derived by this methodology with those estimated in reanalysis models illustrates the well-known underestimate of extreme deep convective systems by global model convective parameterizations (e.g., Schoeberl et al., 2018). A proper representation of these deep convective systems is critical for evaluating the convective influence on TTL H_2O and clouds, and ultimately on the humidity of air entering the stratosphere.

Figure 2 shows the occurrence frequencies of convective cloud top potential temperatures averaged over the Tropics (20°S–20°N) and the Asian (20–40°N, 60–120°E) and North American (10–40°N, 60–120°W) monsoon regions during boreal summer 2007. Also shown is a map of the occurrence frequencies of convective cloud top potential temperatures ≥380 K. Convective clouds over the Asian monsoon region are typically ~5 K higher in altitude than observed elsewhere in the Tropics and subtropics. At least some of this difference may be attributed to the fact that the Asian monsoon convective systems are generally located further north than convection at other longitudes, where isentropes are lower in geometric altitude and the tropopause is higher by ~15 K (asterisks in Figure 2a). The frequent occurrence of deep convection over the Asian monsoon region warrants an investigation of the impact of these convective clouds on the humidity and clouds in the

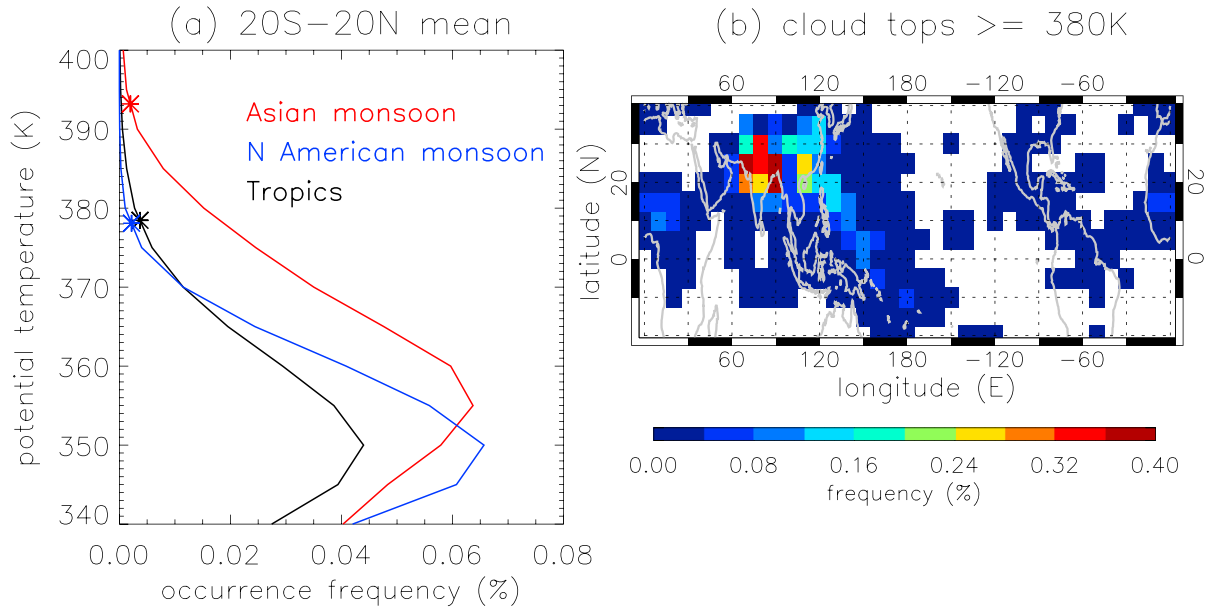

Figure 2. Boreal summer (June–August 2007) mean distributions of satellite-derived convective cloud top occurrence frequencies. (a) Vertical profiles of convective cloud top occurrence frequencies averaged over the Tropics (20°S–20°N; black), Asian (20–40°N, 60–120°E; red), and North American (10–40°N, 60–120°W; blue) monsoon regions. The asterisks denote the mean cold-point tropopause potential temperature averaged over each region. (b) Occurrence frequencies of convective cloud top potential temperature ≥380 K.

globally averaged TTL. In contrast, there are relatively infrequent occurrences of deep convection over the North American monsoon region based on this detection method, in apparent contradiction with some observations (Homeyer et al., 2017; Liu & Liu, 2016; Smith et al., 2017; Solomon et al., 2016); possible explanations of this discrepancy will be discussed in section 4.

Whenever a trajectory intersects a cloud, we saturate the column model up to the cloud top potential temperature. Ice crystals of 30 μm diameter and 100 L^{-1} concentration are also added up to the cloud top potential temperature to simulate the effect of anvil cirrus detrained from deep convection; these anvil cirrus parameters are consistent with observations of anvil cirrus (Jensen et al., 2009). We note that the impact of convection on TTL temperatures (Chae et al., 2011; Selkirk, 1993; Sherwood et al., 2003), which consequently regulate TTL H_2O and clouds, is inherently included, to some degree, in our simulations driven by ERA-Interim temperatures and in the calculation of cloud top altitudes based on a temperature profile of mixed tropopause and environmental air. Using this approach, Ueyama et al. (2015) showed that convection predominantly hydrates the 100-hPa level by ~0.3 ppmv during boreal winter. A similar trajectory study of Schoeberl et al. (2014) showed that convection increases stratospheric-entry H_2O by ~0.5–0.6 ppmv (see Ueyama et al., 2015 for a discussion on the differences between these studies). Both studies found that convectively detrained ice moistens the lower stratosphere by ~10–20% and increases TTL clouds by a factor of 2–3.

3. Results

3.1. H_2O Mixing Ratio at 100 hPa

The 7-day mean MLS H_2O field at the 100-hPa level centered on 3 August 2007 from 10°S to 50°N is shown in Figure 3a. The enhanced H_2O mixing ratios over the Asian and North American monsoon regions are clearly evident, with a monsoon-average H_2O mixing ratio of 5.4 ppmv (compared to the domain-average H_2O mixing ratio of 4.9 ppmv). The driest region is found over the southern equatorial Pacific and the maritime continent with an average H_2O mixing ratio of 4.2 ppmv, which coincide with the region of minimum temperatures at the 100-hPa level (Figure 1) and minimum cold-point tropopause temperatures (not shown). Temperatures are just as cold over southeast Asia and India, but here, air parcels are relatively moist,

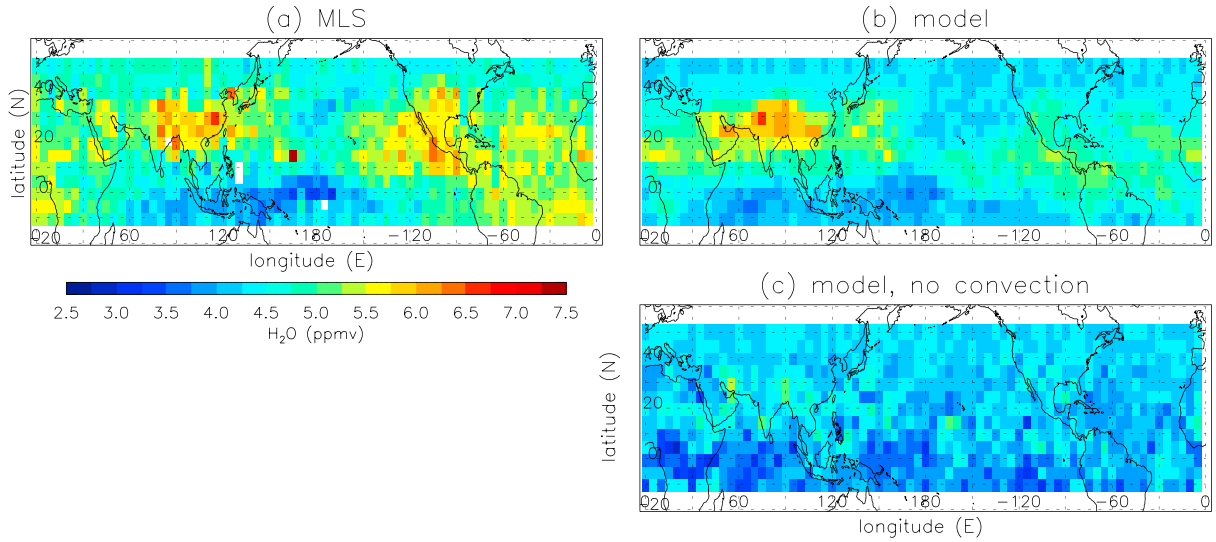

Figure 3. Seven-day mean H_2O mixing ratios at the 100-hPa level centered on 3 August 2007 as (a) observed by Microwave Limb Sounder (MLS; domain average of 4.94 ppmv) and (b) simulated in the model with convection (4.59 ppmv) using all seven sets of trajectories launched on 31 July to 6 August 2007. (c) H_2O mixing ratios at the 100-hPa level on 3 August 2007 simulated in the model without convection (4.11 ppmv) are calculated using a single set of trajectories launched on 3 August 2007. The MLS averaging kernel is applied to the model data (b and c) for comparison with MLS (a).

suggesting that local cold-point temperatures play a minor role in controlling the TTL humidity over these regions. This point will be revisited in section 3.3.

Figure 3b shows the simulated H_2O field at the 100-hPa level on the final day of the trajectories, with MLS averaging kernel applied, averaged over all seven sets of trajectories ending on 31 July to 6 August 2007. The simulated data are also averaged over 5° latitude × 5° longitude grid, and thereby directly comparable to the MLS observation shown in Figure 3a. The simulated field shows a prominent H_2O maximum over the Asian Monsoon region (20–40°N, 60–120°E average of 5.4 ppmv), in excellent agreement with the observations. However, the western hemisphere (i.e., east of the date line) is too dry compared to MLS, which contributes to the overall model dry bias of 0.4 ppmv. In fact, the localized H_2O maximum over the North American monsoon region is virtually absent in the model. This regional dry bias degrades the spatial correlation (r) between the model and MLS fields to ~0.6, with root-mean-square error of ~0.3 ppmv. Possible reasons for the model dry bias over the North American monsoon region are discussed in section 4.

To quantify the impact of convection on the 100-hPa level H_2O, the model was run without convective influence (i.e., without tracing the trajectories through 3-hourly fields of convective cloud top height). The simulated H_2O field with no convection, shown in Figure 3c, lacks any resemblance to MLS observations (r ~0.2) with zonally symmetric structures and a domain average H_2O mixing ratio of 4.1 ppmv. It is evident from the difference plot in Figure 4a that convection moistens the Tropics overall, but predominantly over the Asian monsoon region and equatorial Africa. Although the North American monsoon region is too dry in the model compared to MLS (Figures 3a and 3b), convective moistening is significant across this region and the western hemisphere in general. Thus, our model appears to be underestimating, rather than lacking, the convective influence of parcels in the western hemisphere. Averaged over the 10°S–50°N domain, convection moistens the 100-hPa level by ~0.6 ppmv (or ~15% of the domain average 100-hPa level H_2O mixing ratio in the simulation without convection). Nearly all of the convective moistening is due to the saturating effect of convection, rather than by convectively detrained ice which has a negligible impact on the 100-hPa level H_2O mixing ratio (Table 1).

The role of deep convection on TTL humidity is further investigated by examining the impact of convection with varying cloud top altitudes. Figure 5a shows H_2O mixing ratios at the 100-hPa level averaged over the 10°S–50°N domain in the simulations with convective cloud tops capped at 365, 370, 375, and 380 K potential temperature levels. Over the course of the parcels' 60-day transport into and through the TTL, convective cloud top altitudes >365 K contribute about 0.6 ppmv to the domain-average H_2O mixing ratio at the

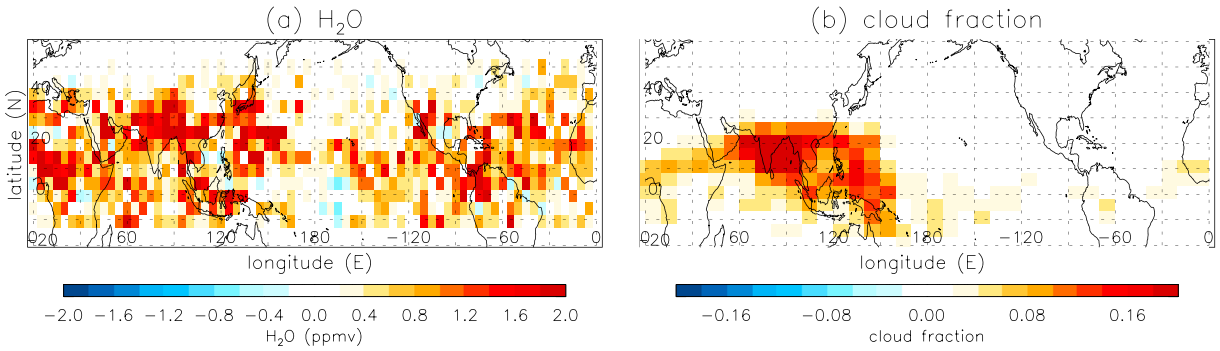

Figure 4. The impact of convection on (a) H_2O mixing ratios at the 100-hPa level and (b) cloud occurrence fraction in the 16–18 km layer. Convective impact on H_2O is calculated as the H_2O difference between simulations with and without convection on the final day of the trajectories (3 August 2007) at the 100-hPa level (not convolved with the Microwave Limb Sounder averaging kernel). Convective impact on the 16–18 km cloud fraction is calculated as the difference in the cloud occurrence statistics calculated over the last 30 days of the 60-day backward trajectories launched on 3 August 2007 (i.e., corresponding to the 4 July to 3 August 2007 time period) between simulations with and without convection.

100-hPa level (i.e., the difference between 4.6 ppmv with all convection and 4.0 ppmv with convection capped at 365 K in Figure 5a). In other words, given that all convection moistens the 10°S–50°N domain at the 100-hPa level by ~0.6 ppmv (Figure 5a and Table 1), convective clouds above 365 K account for almost all (97%) of the total convective moistening at the 100-hPa level. This essentially has to be true with a level of zero radiative heating near 370 K; convection below this level will have insignificant effect at 379 K (~100 hPa). While deep convective systems with cloud tops above 380 K have a relatively small *net* effect on the 100-hPa level humidity (~0.2 ppmv) due to their infrequent occurrences (Figure 2a), these extreme deep convective clouds are significant in that they account for about a third of the total convective moistening at 100 hPa.

We also investigated the impact of Asian monsoon convection by running a simulation that excludes convection within the greater Asian Monsoon region (0–40°N, 40–140°E; magenta box in Figure 6a) where deep convective clouds are most frequently observed (Figure 2). The difference in the domain average 100-hPa H_2O mixing ratios between simulations with and without Asian monsoon convection (Table 1) indicates that

Table 1
Impact of Convection on 100-hPa H_2O and 16–18 km Cloud Fraction

	H_2O [ppmv]	Cloud occurrence [fraction]
All convection	0.61 (15%)	0.040 (169%)
Convectively detrained ice	−0.01	0.009
Convectively detrained ice size increase (*Re* = 15 to 30 μm)	0	−0.002
Convective cloud top altitude adjustment increase (+0.5 to +1.4 km)	0.37	0.017
Convective clouds above 380 K	0.21	0.007
Convective clouds above 375 K	0.34	0.013
Convective clouds above 370 K	0.49	0.025
Convective clouds above 365 K	0.59	0.036
Convection over Asian Monsoon region[a]	0.29	0.022
Convection over Tibetan Plateau[b]	0.10	0.011
Convection over Monsoon region[c]	0.12	0.012
Convection over South Slope[d]	0.13	0.012

Note. The impact of convection on H_2O mixing ratios and cloud occurrence fractions are presented as averages over the 10°S–50°N and 10°S–30°N domain, respectively. Percent differences (in parenthesis) are calculated with respect to the domain average 100-hPa H_2O mixing ratio (3.98 ppmv; not convolved with the Microwave Limb Sounder averaging kernel) and 16–18 km cloud fraction (0.024) in the simulation without convection.
[a]Asian monsoon region is defined as the region 0–40°N, 40–140°E. [b]Tibetan plateau is defined as the area with an elevation of >3 km within 25–40°N, 70–105°E. [c]Monsoon region is defined as the region 10–25°N, 70–105°E. [d]South Slope is defined as the area with an elevation of <3 km within 25–35°N, 70–105°E (see Figure 6 for a map of these regions).

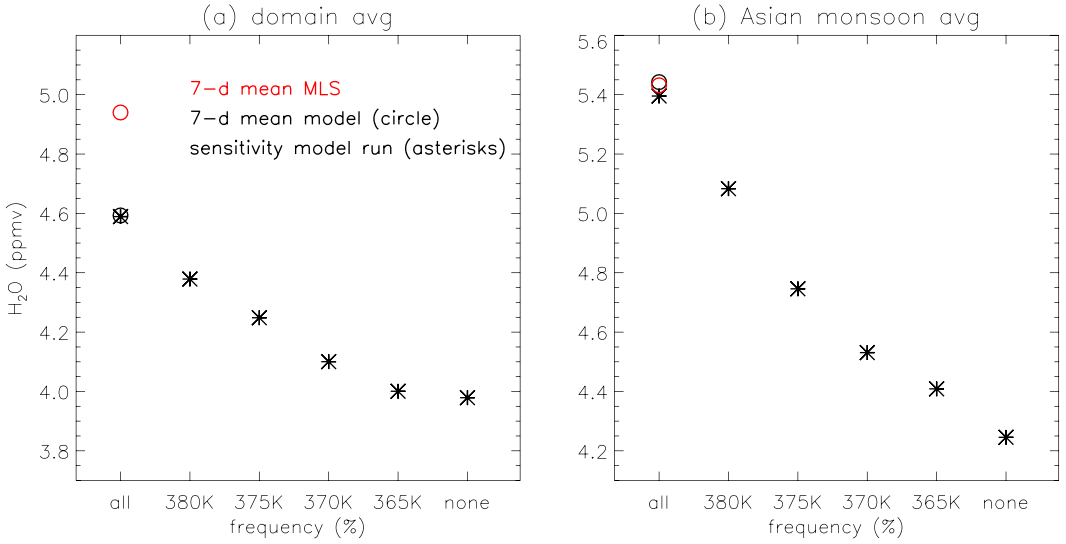

Figure 5. (a) Domain (10°S–50°N) average H_2O mixing ratios at the 100-hPa level on 3 Aug 2007 (final day of the trajectories). The black asterisks represent the mean H_2O mixing ratios for the simulations with all convection ("all"), no convection ("none"), and convective clouds capped at 380, 375, 370, and 365 K potential temperatures. The 7-day (31 July to 6 August 2007) mean H_2O mixing ratios from Microwave Limb Sounder (MLS; red circle) and model data convolved with MLS averaging kernel (black circle) are also shown. (b) As in (a) but averages over the Asian monsoon region (20–40°N, 60–120°E).

Asian monsoon convection contributes approximately 50% (~0.3 ppmv) of the total (global) convective moistening at 100 hPa. Convective sources of H_2O and clouds within the Asian Monsoon region are further investigated in section 3.4.

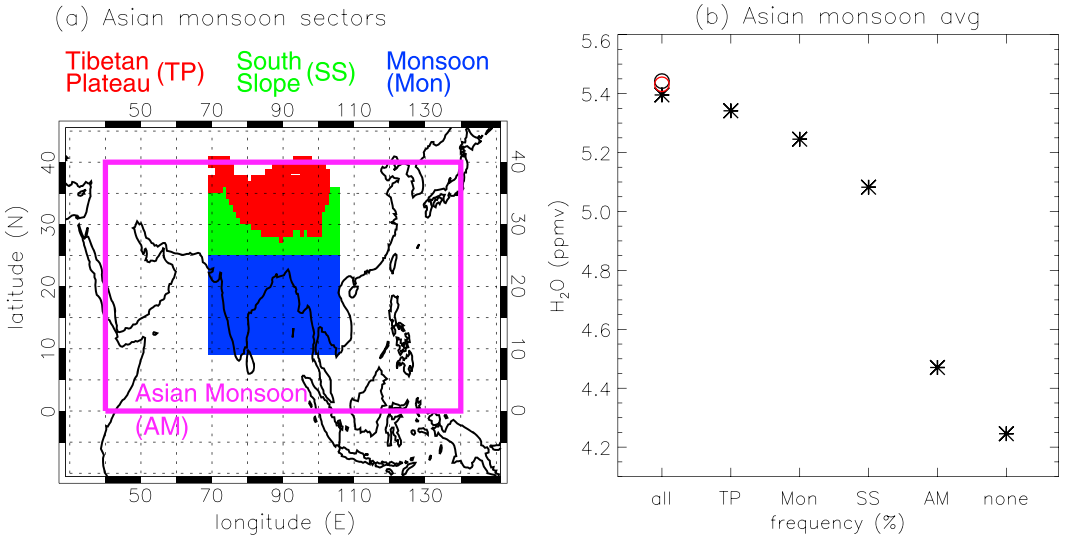

Figure 6. (a) The greater Asian monsoon region (AM; magenta box; 0–40 N°, 40–140°E) and the three sectors defined in this study. The Tibetan Plateau (TP; red) is defined as the area with an elevation of >3 km within 25–40°N and 70–105°E. The South Slope (SS; green) is defined as the area with an elevation of <3 km within 25–35°N and 70–105°E. The monsoon (Mon; blue) is defined as the area within 10–25°N and 70–105°E. The TP, SS, and Mon sectors follow the definition in Fu et al. (2006). (b) Asian monsoon (20–40°N, 60–120°E) average H_2O mixing ratios at the 100-hPa level on 3 August 2007 (final day of the trajectories). The black asterisks represent the mean H_2O mixing ratios for the simulations *excluding* convection over the TP, Mon, SS, and the greater AM regions. The 7-day (31 July to 6 August 2007) mean H_2O mixing ratios from Microwave Limb Sounder (MLS; red circle) and model data convolved with MLS averaging kernel (black circle) are also shown.

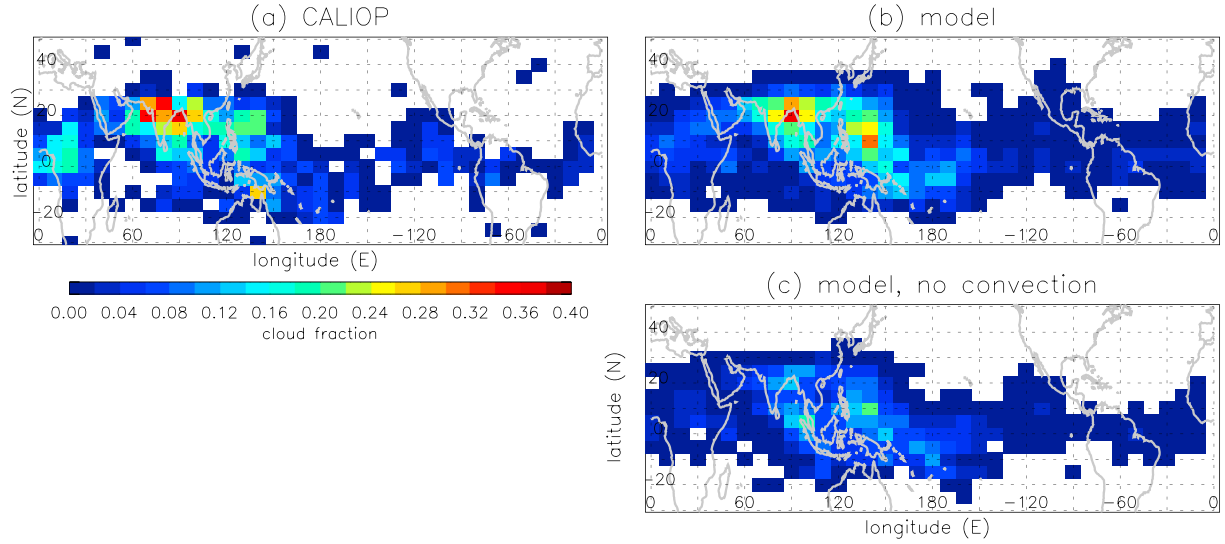

Figure 7. Occurrence fractions of clouds in the 16–18 km pressure altitude layer during 4 Jul to 3 August 2007 (i.e., the last 30 days of the 60-day backward trajectories) as (a) observed by Cloud-Aerosol Lidar with Orthogonal Polarization (10°S–30°N mean cloud fraction of 0.044) and (b) simulated in the model with convection (0.0487) and (c) without convection (0.024). Note that (b) is calculated using all seven sets of trajectories launched on 31 July to 6 August 2007, whereas the sensitivity simulation without convection (c) is calculated using a single set of trajectories launched on 3 August 2007.

3.2. TTL Cloud Occurrence Fraction

The last ~30 days of the 60-day backward trajectory curtain simulations corresponding to the 4 July to 3 August 2007 time period were scanned for cloud occurrences in the 16–18 km layer. For every 5° latitude × 5° longitude grid, the sum of all cloud counts in a grid box was divided by the total number of trajectory passes through that grid box. The resulting cloud occurrence fractions are compared with corresponding cloud statistics based on CALIOP measurements in Figure 7. The simulated and observed distributions are well correlated at r = 0.8, with maximum cloud occurrence fraction over the Asian monsoon region. The model slightly overestimates cloud occurrence in the western tropical Pacific, which could be attributed in part to the sparse sampling of CALIOP measurements.

The vertical profiles of cloud occurrence fraction in the TTL (10°S–30°N) based on CALIOP and model data are shown in Figure 8a. The observed (black) and simulated (red circles) profiles agree reasonably well, with decreasing cloud occurrence fraction from 0.04 to 0.06 at 16 km to nearly zero at 18 km. The model overestimates TTL cloud occurrence in the mid to upper TTL by ~40%, which is primarily associated with the high bias over the western tropical Pacific (Figure 7). In fact, the agreement is excellent over the Asian monsoon region, as shown in Figure 8b.

Cloud fractions are reduced everywhere in the simulation without convection (Figure 7c). The difference from the simulation with convection, shown in Figure 4b, indicates largest enhancements in cloud occurrence over the Asian monsoon region. Averaged over the tropical (10°S–30°N) domain, convection increases the occurrence of mid to upper TTL clouds by ~170% of which more than half is due to deep convection within the Asian monsoon region (Figure 8a and Table 1). Convective impact on clouds is larger in the lower TTL (e.g., ~300% at 15 km; not shown), consistent with the peak in convective cloud top occurrence frequencies at ~350 K potential temperature level (Figure 2a). It is evident from Figure 8 that almost all of the convectively enhanced cloud fraction is due to convective saturation, and not by convectively detrained ice (note the close resemblance between red and gray asterisks profiles corresponding to the cloud fraction profiles of the simulations with and without convectively detrained ice, respectively).

3.3. Locations of Final Dehydration and Convective Hydration

Following Ueyama et al. (2015), we examined the locations of final convection and final in situ cloud formation of parcels, shown in Figure 9. The final convection location is where a parcel is convectively saturated for the last time before arriving at the backward trajectory launch point in the 10°S–50°N domain at ~100 hPa on

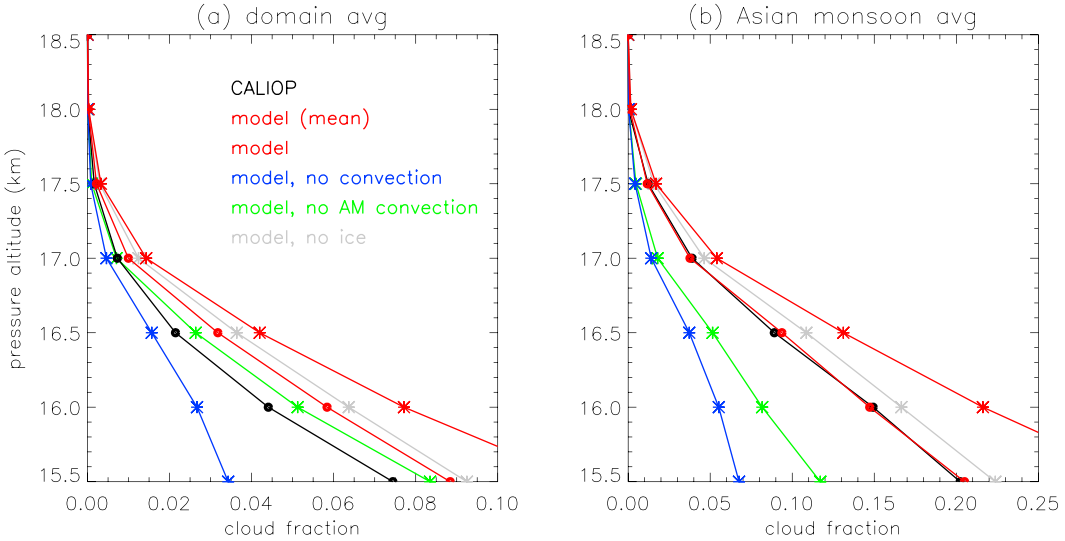

Figure 8. Vertical profiles of cloud occurrence fractions during 4 July to 3 August 2007 (i.e., the last 30 days of the 60-day backward trajectories) averaged over the (a) Tropics (10°S–30°N) and (b) Asian monsoon region (10–30°N, 60–120°E): Cloud-Aerosol Lidar with Orthogonal Polarization observation (black) and simulations with convection (red), no convection (blue), no convection over the Asian monsoon region (green), and no convectively-detrained ice (gray). The mean cloud fraction profile of the simulation with convection using all seven sets of trajectories launched on 31 July to 6 August 2007 are denoted with red circles. The cloud fraction profiles of the sensitivity simulations using a single set of trajectories launched on 3 August 2007 are denoted with asterisks.

3 August 2007. Similarly, the final in situ cloud formation is where a parcel experiences its last ice nucleation event before arriving at the backward trajectory launch point. In a general sense, the final convection and cloud formation locations can be interpreted as the final (re) hydration and dehydration locations of parcels along their trajectories, respectively.

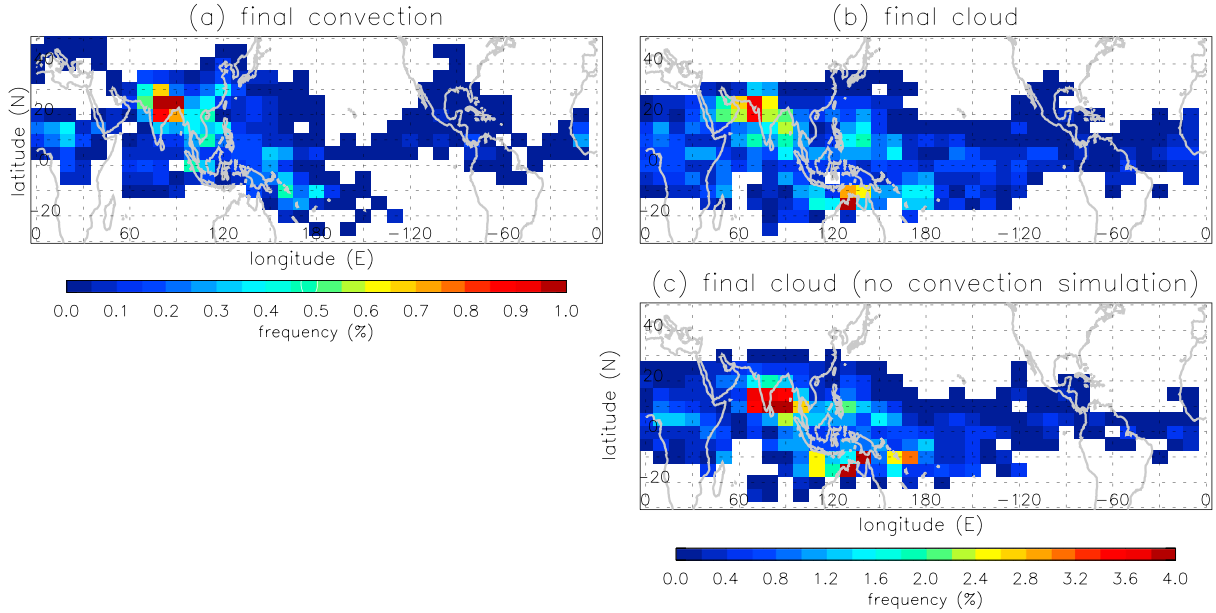

Figure 9. Occurrence frequencies of (a) final convective encounter and (b) final in situ cloud formation of parcels in the 10°S–50°N domain on 3 August 2007. The final convective encounter is the location where a parcel is convectively saturated for the last time before arriving at the backward trajectory launch point in the 10°S–50°N domain on 3 August 2007. The final in situ cloud formation is the location of a parcel's last ice nucleation event before arriving at the backward trajectory launch point. (c) As in (b) but for the simulation with no convection.

More than half (66%) of the parcels at 100 hPa in the 10°S–50°N domain are influenced by convection within the last 60 days with an average time since most recent convection of 25 days. A similar fraction of parcels (58%) is dehydrated by in situ cloud formation with an average time since most recent cloud formation of 21 days. This suggests that convectively influenced parcels are typically dehydrated downstream of convection 4 days later.

The patterns of final convection and in situ cloud formation in Figures 9a and 9b both exhibit a maximum over the Asian monsoon region and broadly resemble the deep convective cloud distribution (Figure 2b) and TTL cloud occurrence distribution (Figure 7), respectively. Parcels are most frequently hydrated by convection in the southern sector of the Asian monsoon anticyclone over the northern Indian subcontinent and subsequently dehydrated downstream following the 100-hPa level flow to the northwest of the minimum temperature region (Figure 1); a more detailed analysis of Asian monsoon air parcels is provided in section 3.4. Northern Australia also appears as one of the preferred regions of final in situ cloud formation, which likely reflects the final dehydration of parcels at the cold tropical tropopause (Figure 1). Compared to the final dehydration events of parcels in the simulation with convection, those of parcels in the simulation without convection occur about 11 days earlier (i.e., average time since most recent cloud formation of 32 days). The spatial pattern of final in situ cloud formation of parcels in the simulation without convection, shown in Figure 9c, closely resembles the 100-hPa temperature pattern (Figure 1), similar to the situation in boreal winter (Ueyama et al., 2015) where the parcel's humidity is primarily set at the cold-point tropopause. During the boreal summer, convection appears to shift the locations of final dehydration northwest of the cold-point tropopause temperature region in the northern Tropics.

3.4. Impact of Convection on the Asian Monsoon Region

As discussed in Sections 3.1 and 3.2 and summarized in Table 1, convection moistens the 100-hPa level by ~0.6 ppmv (~15%) and increases cloud occurrence fraction in the middle to upper TTL by ~170%. Convective impacts are particularly large over the Asian monsoon region, as seen in Figure 4. The H_2O and cloud fields in the simulation without convection exhibit zonally symmetric structures and lack any resemblance to observations. Global convection moistens the Asian monsoon region by ~1.2 ppmv (~30%) at the 100-hPa level and increases cloud occurrence in the mid to upper TTL over the monsoon region by ~195%. Roughly 80% of these regional convective enhancements are driven by convection occurring locally within the Asian monsoon region.

Although there are far fewer deep convective clouds than shallow ones (Figure 2a), the impact of deep convective clouds on the humidity of air at 100 hPa over the Asian monsoon region is as large as the impact of the more frequent, shallower clouds, as demonstrated in Figure 5b. For example, convective cloud top altitudes $>$380 K moisten the regional mean 100-hPa level H_2O by 0.31 ppmv (i.e., the difference between 5.4 ppmv with all convection and 5.1 ppmv with convection capped at 380 K in Figure 5b), which is comparable to the 0.34-ppmv moistening by convective cloud top altitudes in the 375 to 380 K range and larger than the moistening by convective cloud top altitudes in the 370–375 K and 365–370 K ranges (0.21 and 0.12 ppmv, respectively). Similarly, these deep convective clouds have a disproportionately large effect on the middle to upper TTL cloud occurrence over the Asian monsoon region (not shown; e.g., in situ formed cirrus clouds increase 38% by convective clouds $>$380 K versus 21% by convective clouds in the 375–380 K range).

To determine the convective source of H_2O and clouds over the Asian monsoon region, three additional simulations were run in which convection was excluded over the Tibetan Plateau (area with an elevation of $>$3 km within 25–40°N, 70–105°E), South Slope (area with an elevation of $<$3 km within 25–35°N, 70–105°E), and Monsoon region (10–25°N, 70–105°E), respectively (Figure 6a). These monsoon sectors were defined based on the criteria of Fu et al. (2006), who found that convection over the Tibetan Plateau provides the main pathway for cross-tropopause transport of moist air through the Asian monsoon region and into the stratosphere. On the contrary, our results shown in Figure 6b indicate that convection over the Monsoon and South Slope regions has ~3–6 times larger impact on the local 100-hPa humidity over the Asian monsoon region than convection over the Tibetan Plateau. Convective enhancement of TTL cloud occurrence over the Asian Monsoon region is also dominated by convective systems in the South Slope and Monsoon regions (not shown). The global impacts of convection in these three sectors are comparable but lowest for convection over the Tibetan Plateau (Table 1). These results suggest that the convective source of H_2O and clouds

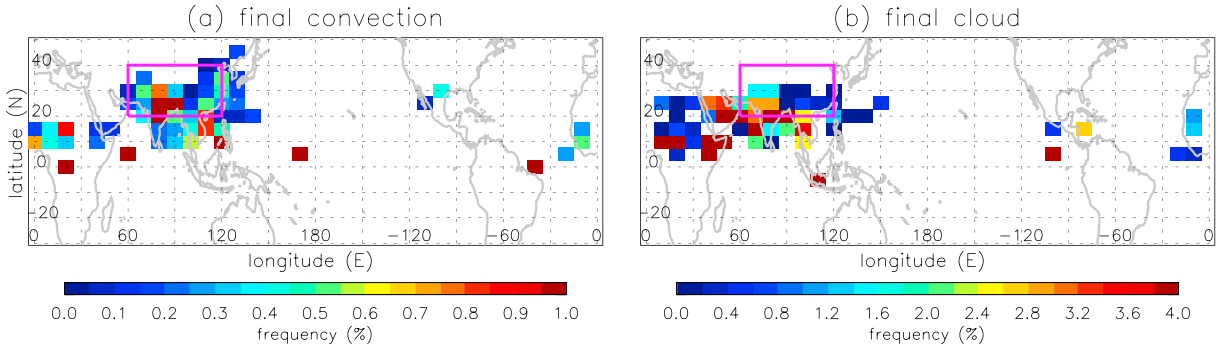

Figure 10. Occurrence frequencies of (a) final convective encounter and (b) final in situ cloud formation of parcels in the Asian monsoon region (magenta box) on 3 August 2007. The final convective encounter is the location where a parcel is convectively saturated for the last time before arriving at the backward trajectory launch point in the Asian monsoon region on 3 August 2007. The final in situ cloud formation is the location of a parcel's last ice nucleation event before arriving at the backward trajectory launch point in the Asian monsoon region.

from the relatively small region to the south of the Tibetan Plateau, including the Bay of Bengal, is the primary contributor to the humidity and cloudiness over the Asian monsoon region.

Figure 10 shows the locations of final convection and final in situ cloud formation of parcels whose backward trajectory launch points reside within the center of the Asian monsoon anticyclone. Approximately 2 weeks prior to 3 August 2007, Asian monsoon parcels are hydrated by convection primarily in the southern sector of the monsoon upper-level anticyclone near the South Slope and Monsoon regions. Within a day following the final convective encounter, parcels are predominantly dehydrated downstream in the southwest sector. Since the typical duration of parcels to circulate around the anticyclone once is about 1–2 weeks, parcels spiral upward in an anticyclonic circulation ~1–2 times before they reach the 100-hPa level. Few parcels are ejected out of the Asian monsoon anticyclone which extends across the tropical African continent (Figure 1), confirming the confined nature of this circulation. The majority (88%) of parcels arriving within the Asian monsoon region at the 100-hPa level are convectively influenced during their 60-day passage through the TTL, which is double the fraction of convectively influenced parcels arriving elsewhere (44%). Additionally, 35% of Asian monsoon parcels are rehydrated by convection *after* final dehydration, as opposed to 10% of parcels outside of the Asian monsoon region. These differences in the history of parcels inside and outside of the Asian monsoon region are consistent with the observed enhancement in 100-hPa H_2O over the Asian monsoon region.

4. Summary and Discussion

The impact of convection on the humidity and clouds in the TTL during boreal summer 2007 is investigated with a focus on the Asian monsoon region. A one-dimensional (vertical), time-dependent cloud microphysical model is used to simulate the nucleation, deposition growth, sedimentation, and sublimation of in situ cirrus clouds and their effects on the humidity profile along backward diabatic trajectories from the 379 K potential temperature (~100-hPa pressure) surface. Convective influence of the parcels is simulated by tracing the trajectories through time-dependent (3-hourly) fields of convective cloud top height based on rainfall measurements, geostationary infrared satellite imagery, and temperature analyses.

The 7-day mean H_2O field centered on 3 August 2007 at the 100-hPa level, convolved with the MLS a priori and averaging kernel, exhibits a pronounced maximum in H_2O over the Asian monsoon region in excellent agreement with MLS observations (Figure 3). The simulated H_2O distribution in the western hemisphere resembles that of observations (i.e., the eastern tropical Pacific, North America, and Atlantic basin are relatively moist compared to the northwest Pacific in the northern subtropical and equatorial latitudes) but is drier than observations by 0.4 ppmv. In particular, the localized H_2O maximum over the North American monsoon region as seen in MLS observations is virtually absent in the model, which degrades the spatial correlation between the simulated and observed H_2O fields ($r = 0.6$). The simulated cloud occurrences in the middle to upper (16–18 km) TTL during 4 July to 3 August 2007 (i.e., the last 30 days of 60-day backward trajectories) are generally in good agreement with those estimated from CALIOP measurements ($r = 0.8$) but are slightly

too high over the western tropical Pacific (Figure 7), effectively overestimating the domain-average cloud occurrence fraction in the middle to upper TTL by ~40% compared to CALIOP observations (Figure 8a). The simulated and observed cloud fractions are in excellent agreement over the Asian monsoon region (Figure 8b).

The impact of convection is quantified by computing the difference between the simulated H_2O mixing ratios and cloud occurrence frequencies with and without convective influence. Averaged over the 10°S–50°N domain, convection moistens the 100-hPa level by ~0.6 ppmv (~15%; Figure 4a), where ~50% of this increase (~0.3 ppmv) is due to the effect of Asian monsoon (0–40°N, 40–140°E) convection. Convection increases tropical (10°S–30°N) mean cloud occurrence in the middle to upper TTL by ~170% (Figure 4b). It is worth noting that while the convective impact on the humidity of the TTL is comparable between boreal winter and summer (both ~15% increase), the convective impact on the upper tropospheric cloud fraction is considerably larger during boreal summer than winter (~30% during winter; Ueyama et al., 2015). On the other hand, Schoeberl et al. (2018) found nearly a doubling (~92%) of the TTL cloud fraction due to convection during boreal winter 2008–2009 using a forward domain filling trajectory model with the same satellite-derived convective cloud top altitude fields used here. We will investigate the differences between these complementary model approaches in a follow-up study to reach closure on the climatological mean impacts of convection on TTL clouds.

Sensitivity simulations with convection capped at various potential temperature levels indicate that extreme deep convective systems have a disproportionately large moistening effect (Figure 5) despite their infrequent occurrence (Figure 2a): averaged over the 10°S–50°N domain, cloud top potential temperatures greater than 380 K account for about a third of the total convective moistening at 100 hPa. This may be because convection penetrating above 380 K transports H_2O above the mean cold-point tropopause and therefore avoids subsequent dehydration. The impact on 100-hPa level humidity by convection whose cloud top potential temperatures exceed 365 K is relatively small (less than 5%).

We have shown that convective moistening is primarily due to the saturating effect of convection; convectively detrained ice crystals have negligible impact on the 100-hPa humidity and upper tropospheric cloud occurrence (Table 1). Our result seemingly contradicts the results of previous studies that have indicated a more significant role of convective ice on TTL and lower stratospheric humidity (Dessler et al., 2016; Schoeberl et al., 2014; Ueyama et al., 2015). We speculate that the effects of convectively detrained ice may largely depend on the ambient relative humidity encountered by the ice crystals during their injection into and transport through the TTL as well as on the details of the convective parameterization, but further analyses are required to explain the variable conclusions on this topic. Details of the convective ice detrainment process and their impact on the TTL will be investigated in a future study.

More than half (66%) of the parcels at the 100-hPa level in the 10°S–50°N domain are convectively hydrated primarily over the northern Indian subcontinent (Figure 9). Final dehydration, as determined by the final in situ cloud formation along trajectories, frequently occurs downstream of convection, so convectively influenced parcels in the Asian monsoon region are more likely to be dehydrated within the monsoon anticyclone than are parcels without convective influence. Unlike during boreal winter, convection appears to shift the locations of final dehydration northwest of the cold temperature region in the Northern Hemisphere Tropics during boreal summer. This suggests a pathway in which moist parcels are able to avoid the lowest-temperature regions of the TTL by remaining inside the anticyclone where temperatures are relatively warm. Typically, Asian monsoon parcels are convectively hydrated in the southern sector of the monsoon upper-level anticyclone and subsequently (within a day) dehydrated downstream in the southwestern sector of the monsoon anticyclone including equatorial Africa (Figure 10). The parcels then spiral upward in the anticyclonic circulation ~1–2 times before arriving at the 100-hPa level.

Convective impact is large over the Asian monsoon region, where H_2O and cloud occurrences are enhanced locally by ~1.2 ppmv (~30%) and ~195%, respectively (Figure 4). The primary source of H_2O and clouds in the Asian monsoon region appears to be from convection south of the Tibetan Plateau in the South Slope and Monsoon regions including the Bay of Bengal (Figure 6), contrary to the findings of Fu et al. (2006) that convection over the Tibetan Plateau is the dominant contributor. We note that Fu et al. (2006) based their conclusions on 3-day backward trajectories, which are not long enough to capture the frequent occurrences of convective hydration over the South Slope and Monsoon regions approximately 2 weeks prior to the parcels

reaching the 100-hPa level within the Asian monsoon anticyclone. The prominent H_2O and cloud maxima within the Asian summer monsoon anticyclone that are evident in observations and simulated in our model with convection are significantly reduced (or virtually absent) in the simulation without convection (Figures 3c and 7c). Therefore, we conclude that convection is the dominant driver of the localized H_2O and cloud maxima in the Asian summer monsoon region. The unique history of air parcels ascending through the TTL and arriving in the Asian monsoon region at the 100-hPa level supports this conclusion: Compared to parcels outside of the Asian monsoon region, Asian monsoon parcels are more likely to be convectively influenced within 60 days (88% versus 44% of parcels outside) and rehydrated by convection *after* final dehydration (35% versus 10% of parcels outside).

Our conclusion regarding the importance of convection on the H_2O enhancement over the Asian summer monsoon region contradicts the trajectory modeling studies of James et al. (2008) and Schoeberl et al. (2013), who found a relatively small effect of convection on the lower stratospheric H_2O over the Asian monsoon region. The reason for the discrepancy may be related to the different modeling approaches. Schoeberl et al. (2013) not only assume instantaneous dehydration when the relative humidity exceeds 100% but also ignore the convective influence of parcels along forward domain-filling trajectories. The fact that their model simulates enhanced H_2O over the Asian and North American monsoon regions (see their Figure 2) even without explicit treatment of convective influence suggests that their results may be sensitive to the parcel initialization with 50-ppmv H_2O above the local zero radiative heating level. We note that the zero radiative heating level is high (~370 K) over the monsoon regions. To investigate this possibility, we initialized our model with 25 ppmv above the level of zero radiative heating and calculated the H_2O profiles along parcel trajectories while excluding convection and detailed microphysical processes. The resulting 100-hPa level H_2O field (not shown) resembles that of Schoeberl et al. (2013), which suggests that the enhanced H_2O over the monsoon regions presented in Schoeberl et al. (2013) is at least partially related to the initialization of moist parcels at relatively high altitudes.

The explanation of the difference between our results indicating the predominant effect of convection on TTL humidity over the Asian monsoon region and the relatively small impact of convective moistening (0.3 ppmv) found by James et al. (2008) is less clear. James et al. (2008) assume complete fall-out of ice crystals when the relative humidity of a parcel exceeds a predetermined threshold, whereas our study uses a cloud microphysical model to simulate the nucleation, deposition growth, sedimentation, and sublimation processes in combination with wave-induced temperature variability (Kim & Alexander, 2015). Another difference between our approaches is that James et al. (2008) use 3-hourly radiative heating rates from ERA-Interim, whereas our trajectories are calculated using seasonal mean, offline calculations of observation-based heating rates from Yang et al. (2010). The level of zero radiative heating is at a higher (+1.5 km) altitude, and the ascent above that level is ~50% weaker in the Yang et al. (2010) data set compared to those of ERA-Interim. Sensitivity experiments show that detailed microphysical processes moisten the 100-hPa level by ~0.9 ppmv (e.g., by sublimation of falling ice crystals), while wave-driven temperature variability dehydrates by ~0.3 ppmv (not shown). Using seasonal mean Yang et al. (2010) heating rates as opposed to seasonal mean ERA-Interim heating rates dehydrates by ~0.2 ppmv, while using seasonal mean ERA-Interim heating rates as opposed to 6-hourly ERA-Interim heating rates moistens by ~0.05 ppmv (not shown). The proper treatment of waves and heating rates are unlikely to influence the effect of convection on TTL humidity, but convective impact may be reduced if instantaneous fall-out of condensate is assumed, as in James et al. (2008). The different convective cloud top data sources of the studies could also contribute to the different results.

Based on MLS H_2O measurements, outgoing longwave radiation data (as a proxy for deep convection), and ERA-Interim meteorological analyses, Randel et al. (2015) found that stronger (weaker) convection cools the subtropical lower stratosphere more (less) efficiently and leads to a relatively dry (wet) stratosphere. Thus, they concluded that the localized H_2O maxima in the Asian and North American monsoon regions during boreal summer are mainly controlled by large-scale circulation and temperatures, rather than by deep convection. Our results are seemingly at odds with their findings, but Randel et al. (2015) results are pertinent for understanding the modulation of *subseasonal variations* in lower stratospheric H_2O while our study provides insights on the fundamental driver of the *seasonal mean* H_2O over the summer monsoon regions. In this study, the cooling effect of convection is accounted for by modifying the temperature profile above the

tropopause when calculating the convective cloud top altitudes (as described in section 2), but the time-height curtains of temperature used to drive the cloud processes are not altered. Our model setup is not suitable for testing the Randel et al. (2015) hypothesis, but we suspect that the cooling effect of convection in our model yields similar tendencies in the local humidity field on a day-to-day time scale, in agreement with their study.

We have not investigated the impact of convection on the North American monsoon region because our model simulations do not produce the H_2O and cloud maxima in the western hemisphere that are apparent in the observations. Both aircraft measurements and MLS retrievals show evidence for anomalously high H_2O over North America in the lowermost stratosphere during the monsoon season (Hanisco et al., 2007; Schwartz et al., 2013; Smith et al., 2017). These H_2O enhancements are undoubtedly associated with convection over North America that extends deep into the boreal summer stratosphere (Homeyer et al., 2017; Liu & Liu, 2016; Smith et al., 2017; Solomon et al., 2016). Our representation of convection may not produce cloud top potential temperatures that are high enough over North America to sufficiently moisten the lowermost stratosphere for two reasons. First, although our convective influence approach will identify extensive convective anvils, the occurrence of the overshoots into the very dry stratosphere with low relative humidity can be underestimated because of the rapid sublimation of ice crystals (leaving minimal cloud for detection by infrared satellite measurements). Second, our cloud mixing scheme above the local tropopause likely underestimates the fraction of stratospheric air in the convective plumes in high shear environments. In such cases, convective cloud top potential temperatures will be underestimated (Homeyer et al., 2017), even if convective cloud top *altitudes* are not. We examined the sensitivity to the infrared adjustment altitude by running two additional simulations that bracket the probable range of the adjustment altitude (+0.5 and +1.4 km). Although the H_2O and cloud occurrence in the North American monsoon region are enhanced in the simulation with convective cloud top height adjustment of +1.4 km, they are still lower than observations, and the H_2O and clouds elsewhere (including the Asian monsoon region) are now much too high (not shown). The average uncertainty associated with the convective cloud top altitude adjustment is ~0.4 ppmv (~9%) for H_2O and ~0.02 (~70%) for cloud occurrence fraction (Table 1). The aforementioned explanations of why our methodology may underestimate the convective cloud top potential temperatures over North America are not likely to be relevant over the Asian monsoon where the TTL relative humidity and tropopause potential temperatures are higher, but further analysis is needed to characterize the detailed convective processes in these two monsoon regions and assess their impact on the local TTL. Sensitivities to additional convective parameters and improvements to the estimation of convective cloud top altitudes are currently being investigated.

Our results imply the need for accurate representations of convection and TTL cirrus physical properties in global models to adequately simulate future trends in stratospheric humidity in a changing climate. TTL processes occurring over the Asian monsoon region are particularly important for the humidity control in boreal summertime. In contrast to many previous studies, we find that convectively detrained ice crystals are not important for controlling TTL humidity and clouds during boreal summer. A potential explanation for the different conclusions is the use of observation-based convection (such as the one used in this study) versus parameterized convection in global models. We argue that the latter poorly represents deep convective clouds in the upper TTL, which are critically important for controlling the humidity and clouds near the tropopause region, and ultimately the humidity of the stratosphere. Future work will investigate the climatological mean and variability of the convective influence on the humidity of air entering the tropical lower stratosphere.

Acknowledgments
We thank two anonymous reviewers who provided constructive reviews and suggestions. We thank the Aura Science Team for the MLS data (http://mls.jpl.nasa.gov/), the CALIPSO science team for the cloud profile data (https://eosweb.larc.nasa.gov/project/calipso/calipso_table), and the ECMWF for the ERA-Interim data (http://apps.ecmwf.int/datasets/data/interim_full_daily/). Convection data set used in this study is available through L. Pfister (leonhard.pfister@nasa.gov) at https://bocachica.arc.nasa.gov/~lpfister/cloudtop/. This work was supported by the NASA Aura Science Team and Atmospheric Composition Modeling and Analysis Program and NASA Upper Atmosphere Composition Observations Program.

References

Bannister, R. N., O'Neill, A., Gregory, A. R., & Nissen, K. M. (2004). The role of the south-east Asian monsoon and other seasonal features in creating the 'tape-recorder' signal in the unified model. *Quarterly Journal of the Royal Meteorological Society*, *130*, 1531–1554. https://doi.org/10.1256/qj.03.106

Bergman, J. W., Jensen, E. J., Pfister, L., & Bui, T. V. (2016). Air parcel trajectory dispersion near the tropical tropopause. *Journal of Geophysical Research*, *121*, 3759–3775. https://doi.org/10.1029/2015JD024320

Bergman, J. W., Jensen, E. J., Pfister, L., & Yang, Q. (2012). Seasonal differences of vertical-transport efficiency in the tropical tropopause layer: On the interplay between tropical deep convection, large-scale vertical ascent, and horizontal circulations. *Journal of Geophysical Research*, *117*, D05302. https://doi.org/10.1029/2011JD016992

Bonazzola, M., & Haynes, P. H. (2004). A trajectory-based study of the tropical tropopause region. *Journal of Geophysical Research*, *109*, D20112. https://doi.org/10.1029/2003JD004356

Chaboureau, J.-P., Cammas, J.-P., Duron, J., Mascart, P. J., Sitnikov, N. M., & Voessing, H.-J. (2007). A numerical study of tropical cross-tropopause transport by convective overshoots. *Atmospheric Chemistry and Physics*, *7*(7), 1731–1740. https://doi.org/10.5194/acp-7-1731-2007

Chae, J. H., Wu, D. L., Read, W. G., & Sherwood, S. C. (2011). The role of tropical deep convective clouds on temperature, water vapor, and dehydration in the tropical tropopause layer (TTL). *Atmospheric Chemistry and Physics*, *11*(8), 3811–3821. https://doi.org/10.6194/acp-11-3811-2011

Corti, T., Luo, B. P., de Reus, M., Brunner, D., Cairo, F., Mahoney, M. J., et al. (2008). Unprecedented evidence for deep convection hydrating the tropical stratosphere. *Geophysical Research Letters*, *35*, L10810. https://doi.org/10.1029/2008GL033641

Corti, T., Luo, B. P., Fu, Q., Vömel, H., & Peter, T. (2006). The impact of cirrus clouds on tropical troposphere-to-stratosphere transport. *Atmospheric Chemistry and Physics*, *6*(9), 2539–2547. https://doi.org/10.5194/acp-6-2539-2006

Danielsen, E. F. (1993). In situ evidence of rapid, vertical, irreversible transport of lower tropospheric air into the lower tropical stratosphere by convective cloud turrets and by larger-scale upwelling in tropical cyclones. *Journal of Geophysical Research*, *98*, 8665–8681. https://doi.org/10.1029/92JD02954

Dee, D. P., Uppala, S. M., Simmons, A. J., Berrisford, P., Poli, P., Kobayashi, S., et al. (2011). The ERA-Interim reanalysis: Configuration and performance of data assimilation system. *Quarterly Journal of the Royal Meteorological Society*, *137*(656), 553–597. https://doi.org/10.1002/qj.828

Dessler, A. E., Hanisco, T. F., & Fueglistaler, S. (2007). Effects of convective ice lofting on H_2O and HDO in the tropical tropopause layer. *Journal of Geophysical Research*, *112*, D18309. https://doi.org/10.1029/2007JD008609

Dessler, A. E., & Sherwood, S. C. (2004). Effect of convection on the summertime extratropical lower stratosphere. *Journal of Geophysical Research*, *109*, D23301. https://doi.org/10.1029/2004JD005209

Dessler, A. E., Ye, H., Wang, T., Schoeberl, M. S., Oman, L. D., Douglass, A. R., et al. (2016). Transport of ice into the stratosphere and the humidification of the stratosphere over the 21st century. *Geophysical Research Letters*, *43*, 2323–2329. https://doi.org/10.1002/2016GL067991

Devasthale, A., & Fueglistaler, S. (2010). A climatological perspective of deep convection penetrating the TTL during the Indian summer monsoon from the AVHRR and MODIS instruments. *Atmospheric Chemistry and Physics*, *10*(10), 4573–4582. https://doi.org/10.5194/acp-10-4573-2010

Dinh, T., & Fueglistaler, S. (2014). Microphysical, radiative, and dynamical impacts of thin cirrus clouds on humidity in the tropical tropopause layer and lower stratosphere. *Geophysical Research Letters*, *41*, 6949–6955. https://doi.org/10.1002/2014GL061289

Dinh, T., Podglajen, A., Hertzog, A., Legras, B., & Plougonven, R. (2016). Effect of gravity wave temperature fluctuations on homogeneous ice nucleation in the tropical tropopause layer. *Atmospheric Chemistry and Physics*, *16*(1), 35–46. https://doi.org/10.5194/acp-16-35-2016

Fu, R., Hu, Y., Wright, J. S., Jiang, J. H., Dickinson, R. E., Chen, M., et al. (2006). Short circuit of water vapor and polluted air to the global stratosphere by convective transport over the Tibetan Plateau. *Proceedings of the National Academy of Sciences of the United States of America*, *103*(15), 5664–5669. https://doi.org/10.1073/pnas.0601584103

Fueglistaler, S., & Baker, M. B. (2006). A modeling study of the impact of cirrus clouds on the moisture budget of the upper troposphere. *Atmospheric Chemistry and Physics*, *6*(5), 1425–1434. https://doi.org/10.5194/acp-6-1425-2006

Fueglistaler, S., Bonazzola, M., Haynes, P. H., & Peter, T. (2005). Stratospheric water vapor predicted from the Lagrangian temperature history of air entering the stratosphere in the tropics. *Journal of Geophysical Research*, *110*, D08107. https://doi.org/10.1029/2004JD005516

Fueglistaler, S., Dessler, A. E., Dunkerton, T. J., Folkins, I., Fu, Q., & Mote, P. W. (2009). Tropical tropopause layer. *Reviews of Geophysics*, *47*, RG1004. https://doi.org/10.1029/2008RG00267

Gettelman, A., Birner, T., Eyring, V., Akiyoshi, H., Bekki, S., Brühl, C., et al. (2009). The tropical tropopause layer 1960–2100. *Atmospheric Chemistry and Physics*, *9*(5), 1621–1637. https://doi.org/10.5194/acp-9-1621-2009

Gettelman, A., Hegglin, M. I., Son, S.-W., Kim, J., Fujiwara, M., Birner, T., et al. (2010). Multimodel assessment of the upper troposphere and lower stratosphere: Tropics and global trends. *Journal of Geophysical Research*, *115*, D00M08. https://doi.org/10.1029/2009JD013638

Gettelman, A., Kinnison, D. E., Dunkerton, T. J., & Brasseur, G. P. (2004). Impact of monsoon circulations on the upper troposphere and lower stratosphere. *Journal of Geophysical Research*, *109*, D22101. https://doi.org/10.1029/2004JD004878

Gettelman, A., Randel, W. J., Wu, F., & Massie, S. T. (2002). Transport of water vapor in the tropical tropopause layer. *Geophysical Research Letters*, *29*(1), 1009. https://doi.org/10.1029/2001GL013818

Grosvenor, D. P., Choularton, T. W., Coe, H., & Held, G. (2007). A study of the effect of overshooting deep convection on the water content of the TTL and lower stratosphere from cloud resolving model simulations. *Atmospheric Chemistry and Physics*, *7*(18), 4977–5002. https://doi.org/10.5194/acp-7-4977-2007

Hanisco, T. F., Moyer, E. J., Weinstock, E. M., St. Clair, J. M., Sayres, D. S., Smith, J. B., et al. (2007). Observations of deep convective influence on stratospheric water vapor and its isotopic composition. *Geophysical Research Letters*, *34*, L04814. https://doi.org/10.1029/2006GL027899

Hartmann, D. L., Holton, J. R., & Fu, Q. (2001). The heat balance of the tropical tropopause, cirrus, and stratospheric dehydration. *Geophysical Research Letters*, *28*, 1969–1972. https://doi.org/10.1029/2000GL012833

Homeyer, C. R., McAuliffe, J. D., & Bedka, K. M. (2017). On the development of above-anvil cirrus plumes in extratropical convection. *Journal of the Atmospheric Sciences*, *74*(5), 1617–1633. https://doi.org/10.1175/JAS-D-16-0269.1

James, R., Bonazzola, M., Legras, B., Surbled, K., & Fueglistaler, S. (2008). Water vapor transport and dehydration above convective outflow during Asian monsoon. *Geophysical Research Letters*, *35*, L20810. https://doi.org/10.1029/2008GL035441

Jensen, E. J., Lawson, P., Baker, B., Pilson, B., Mo, Q., Heymsfield, A. J., et al. (2009). On the importance of small ice crystals in tropical anvil cirrus. *Atmospheric Chemistry and Physics*, *9*(15), 5519–5537. https://doi.org/10.5194/acp-9-5519-2009

Jensen, E. J., & Pfister, L. (2004). Transport and freeze-drying in the tropical tropopause layer. *Journal of Geophysical Research*, *109*, D02207. https://doi.org/10.1029/2003JD004022

Jensen, E. J., Pfister, L., & Toon, O. B. (2011). Impact of radiative heating, wind shear, temperature variability, and microphysical processes on the structure and evolution of thin cirrus in the tropical tropopause layer. *Journal of Geophysical Research*, *116*, D12209. https://doi.org/10.1029/2010JD015417

Kim, J.-E., & Alexander, M. J. (2013). A new wave scheme for trajectory simulations of stratospheric water vapor. *Geophysical Research Letters*, *40*, 5286–5290. https://doi.org/10.1002/grl.50963

Kim, J.-E., & Alexander, M. J. (2015). Direct impacts of waves on tropical cold point tropopause temperature. *Geophysical Research Letters*, *42*(5), 1584–1592. https://doi.org/10.1002/2014.GL062737

Kley, D., Schmeltekopf, A. L., Kelly, K., Winker, R. H., Thomspon, T. L., & McFarland, M. (1982). Transport of water through the tropical tropopause. *Geophysical Research Letters*, *9*, 617–620. https://doi.org/10.1029/GL009i006p00617

Koop, T., Luo, B., Tsias, A., & Peter, T. (2000). Water activity as the determinant for homogeneous ice nucleation in aqueous solutions. *Nature*, *406*(6796), 611–614. https://doi.org/10.1038/35020537

Kritz, M. A., Rosner, S. W., Kelly, K. K., Loewenstein, M., & Chan, K. R. (1993). Radon measurements in the lower tropical stratosphere: Evidence for rapid vertical transport and dehydration of tropospheric air. *Journal of Geophysical Research*, *98*, 8725–8736. https://doi.org/10.1029/92JD02524

Lelieveld, J., Brühl, C., Jöckel, P., Steil, B., Crutzen, P., Fischer, H., et al. (2007). Stratospheric dryness: Model simulations and satellite observations. *Atmospheric Chemistry and Physics*, *7*(5), 1313–1332. https://doi.org/10.5194/acp-7-1313-2007

Liu, N., & Liu, C. (2016). Global distribution of deep convection reaching tropopause in 1 year GPM observations. *Journal of Geophysical Research: Atmospheres*, *121*, 3824–3842. https://doi.org/10.1002/2015JD024430

Liu, Y. S., Fueglistaler, S., & Haynes, P. H. (2010). Advection-condensation paradigm for stratospheric water vapor. *Journal of Geophysical Research*, *115*, D24307. https://doi.org/10.1029/2010JD014352

Minnis, P., Yost, C. R., Sun-Mack, S., & Chen, Y. (2008). Estimating the top altitude of optically thick ice clouds from thermal infrared satellite observations using CALIPSO data. *Geophysical Research Letters*, *35*, L12801. https://doi.org/10.1029/2008GL033847

Mote, P. W., Rosenlof, K. H., McIntyre, M. E., Carr, E. S., Gille, J. C., Holton, J. R., et al. (1996). An atmospheric tape-recorder: The imprint of tropical tropopause temperatures on stratospheric water vapor. *Journal of Geophysical Research*, *101*, 3989–4006. https://doi.org/10.1029/95JD03422

Park, M., Randel, W. J., Gettelman, A., Massie, S. T., & Jiang, J. H. (2007). Transport above the Asian summer monsoon anticyclone inferred from Aura Microwave Limb Sounder tracers. *Journal of Geophysical Research*, *112*, D16309. https://doi.org/10.1029/2006JD008294

Pfister, L., Scott, S., Loewenstein, M., Bowen, S., & Legg, M. (1993). Mesoscale disturbances in the tropical stratosphere excited by convection: Observations and effects on the stratospheric momentum budget. *Journal of the Atmospheric Sciences*, *50*(8), 1058–1075. https://doi.org/10.1175/1520-0469(1993)050%3C1058:MDITTS%3E2.0.CO;2

Pfister, L., Selkirk, H. B., Jensen, E. J., Schoeberl, M. R., Toon, O. B., Browell, E. V., et al. (2001). Aircraft observations of thin cirrus clouds near the tropical tropopause. *Journal of Geophysical Research*, *106*, 9765–9786. https://doi.org/10.1029/2000JD900648

Randel, W. J., & Jensen, E. J. (2013). Physical processes in the tropical tropopause layer and their roles in a changing climate. *Nature Geoscience*, *6*(3), 169–176. https://doi.org/10.1038/ngeo1733

Randel, W. J., Wu, F., Gettelman, A., Russell, J. M. III, Zawodny, J. M., & Oltmans, S. J. (2001). Seasonal variation of water vapor in the lower stratosphere observed in Halogen Occultation Experiment data. *Journal of Geophysical Research*, *106*, 14,313–14,325. https://doi.org/10.1029/2001JD900048

Randel, W. J., Wu, F., Vömel, H., Nedoluha, G. E., & Forster, P. (2006). Decreases in stratospheric water vapor after 2001: Links to changes in the tropical tropopause and the Brewer-Dobson circulation. *Journal of Geophysical Research*, *111*, D12312. https://doi.org/10.1029/2005JD006744

Randel, W. J., Zhang, K., & Fu, R. (2015). What controls stratospheric water vapor in the NH summer monsoon regions? *Journal of Geophysical Research: Atmospheres*, *120*, 7988–8001. https://doi.org/10.1002/2015JD023622

Read, W. G., Lambert, A., Bacmeister, J., Cofield, R. E., Christensen, L. E., Cuddy, D. T., et al. (2007). Aura Microwave Limb Sounder upper tropospheric and lower stratospheric H_2O and relative humidity with respect to ice validation. *Journal of Geophysical Research*, *112*, D24S35. https://doi.org/10.1029/2007JD008752

Schiller, C., Grooβ, J.-U., Konopka, P., Plöger, F., Silva dos Santos, F. H., & Spelten, N. (2009). Hydration and dehydration at the tropical tropopause. *Atmospheric Chemistry and Physics*, *9*(24), 9647–9660. https://doi.org/10.5194/acp-9-9647-2009

Schoeberl, M. R., Dessler, A., & Wang, T. (2013). Modeling upper tropospheric and lower stratospheric water vapor anomalies. *Atmospheric Chemistry and Physics*, *13*(15), 7783–7793. https://doi.org/10.5194/acp-13-7783-2013

Schoeberl, M. R., Dessler, A., Wang, T., Avery, M., & Jensen, E. J. (2014). Cloud formation, convection, and stratospheric dehydration. *Earth and Space Science*, *1*, 1–17. https://doi.org/10.1002/2014EA000014

Schoeberl, M. R., Dessler, A., Ye, H., Wang, T., Avery, M., & Jensen, E. (2016). The impact of gravity waves and cloud nucleation threshold on stratospheric water and tropical tropospheric cloud fraction. *Earth and Space Science*, *3*, 295–305. https://doi.org/10.1002/2016EA000180

Schoeberl, M. R., & Dessler, A. E. (2011). Dehydration of the stratosphere. *Atmospheric Chemistry and Physics*, *11*(16), 8433–8446. https://doi.org/10.5194/acp-11-8433-2011

Schoeberl, M. R., Jensen, E., Pfister, L., Ueyama, R., Avery, M., & Dessler, A. E. (2018). Convective hydration of the upper troposphere and lower stratosphere. *Journal of Geophysical Research: Atmospheres*, *123*, 4583–4593. https://doi.org/10.1029/2018JD028286

Schoeberl, M. R., Jensen, E. J., & Woods, S. (2015). Gravity waves amplify upper tropospheric dehydration by clouds. *Earth and Space Science*, *2*, 485–500. https://doi.org/10.1002/2015EA000127

Schwartz, M. J., Read, W. G., Santee, M. L., Livesey, N. J., Froidevaux, L., Lambert, A., & Manney, G. L. (2013). Convectively injected water vapor in the North American summer lowermost stratosphere. *Geophysical Research Letters*, *40*, 2316–2321. https://doi.org/10.1002/grl.50421

Selkirk, H. B. (1993). The tropopause cold trap in the Australian monsoon during STEP/AMEX 1987. *Journal of Geophysical Research*, *98*, 8591–8610. https://doi.org/10.1029/92JD02932

Sherwood, S. C., Chae, J.-H., Minnis, P., & McGill, M. (2004). Underestimation of deep convective cloud tops by thermal imagery. *Geophysical Research Letters*, *31*, L11102. https://doi.org/10.1029/2004GL019699

Sherwood, S. C., & Dessler, A. E. (2001). A model for transport across the tropical tropopause. *Journal of the Atmospheric Sciences*, *58*, 765–779.

Sherwood, S. C., Horinouchi, T., & Zelenzik, H. A. (2003). Convective impact on temperatures observed near the tropical tropopause. *Journal of the Atmospheric Sciences*, *60*, 1847–1856. https://doi.org/10.1175/1520-0469(2003)060%3C1847:CIOTON%3E2.0.CO;2

Smith, J. B., Wilmouth, D. M., Bedka, K. M., Bowman, K. P., Homeyer, C. R., Dykema, J. A., et al. (2017). A case study of convectively sourced water vapor observed in the overworld stratosphere over the United States. *Journal of Geophysical Research: Atmospheres*, *122*, 9529–9554. https://doi.org/10.1002/2017JD026831

Solomon, D. L., Bowman, K. P., & Homeyer, C. R. (2016). Tropopause-penetrating convection from three-dimensional gridded NEXRAD data. *Journal of Applied Meteorology and Climatology*, *55*(2), 465–478. https://doi.org/10.1175/JAMC-D-15-0190.1

Tissier, A.-S., & Legras, B. (2016). Convective sources of trajectories traversing the tropical tropopause layer. *Atmospheric Chemistry and Physics*, *16*(5), 3383–3398. https://doi.org/10.5194/acp-16-3383-2016

Ueyama, R., Jensen, E. J., Pfister, L., Diskin, G. S., Bui, T. P., & Dean-Day, J. M. (2014). Dehydration in the tropical tropopause layer: A case study for model evaluation using aircraft observations. *Journal of Geophysical Research: Atmospheres*, *119*, 5299–5316. https://doi.org/10.1002/2013JD021381

Ueyama, R., Jensen, E. J., Pfister, L., & Kim, J.-E. (2015). Dynamical, convective, and microphysical control on wintertime distributions of water vapor and clouds in the tropical tropopause layer. *Journal of Geophysical Research: Atmospheres*, *120*, 10,483–10,500. https://doi.org/10.1002/2015JD023318

Winker, D. M., Vaughan, M. A., Omar, A., Hu, Y., Powell, K. A., Liu, Z., et al. (2009). Overview of the CALIPSO mission and CALIOP data processing algorithms. *Journal of Atmospheric and Oceanic Technology*, *26*(11), 2310–2323. https://doi.org/10.1175/2009JTECHA1281.1

Wright, J. S., Fu, R., Fueglistaler, S., Liu, Y. S., & Zhang, Y. (2011). The influence of summertime convection over Southeast Asia on water vapor in the tropical stratosphere. *Journal of Geophysical Research*, *116*, D12302. https://doi.org/10.1029/2010JD015416

Yang, Q., Fu, Q., & Hu, Y. (2010). Radiative impacts of clouds in the tropical tropopause layer. *Journal of Geophysical Research*, *115*, D00H12. https://doi.org/10.1029/2009JD012393